GEOPHYSICS, VOL. 69, NO. 6 (NOVEMBER-DECEMBER 2004); P. 1387–1393, 12 FIGS.
10.1190/1.1836813

Electromagnetic detection of buried metallic objects using quad–quad conductivity

Haoping Huang[1] and I. J. Won[1]

ABSTRACT

Apparent conductivity computed from in-phase and quadrature components has been used successfully to detect buried metallic objects such as unexploded ordnance (UXO). The conductivity computation uses magnetic susceptibility calculated from the lowest-frequency in-phase data obtained at a specific sensor height. Over magnetic soils, however, the in-phase component may fluctuate with varying sensor heights. Uncertainties in sensor height, common with handheld or cart-mounted sensors in rough terrain, can produce errors in the computed magnetic susceptibility, which, in turn, causes errors in apparent conductivity.

To overcome these limitations, we have developed an algorithm to compute the quad–quad apparent conductivity from the quadrature components at two frequencies. Our results show that the quad–quad technique has several advantages for detecting metal targets in magnetic terrains: it is (1) insensitive to the magnetic polarization currents; (2) it is immune to sensor motion over magnetic soil; and (3) it is biased to metal objects and can detect small and/or deep metal targets. The first two properties suppress the noise caused by magnetic terrain and sensor motion and thus yield a quiet background. The last property emphasizes metal objects as sought anomalies over geologic variations.

INTRODUCTION

Frequency-domain electromagnetic (EM) sensors can be used as a conductivity meter, as well as an active magnetometer, when they operate at sufficiently low frequencies (Huang and Won, 2000; Won and Huang, 2004). This duality allows us to separate responses from a conductive target, such as unexploded ordnance (UXO), from those caused by magnetic soils. The apparent conductivity computed from the in-phase I and quadrature Q components has been used successfully to recognize anomalies caused by metal objects buried in magnetic terrain (Huang and Won, 2003a,b,c). It is well known that the magnetic susceptibility of soils greatly impacts the I-component but has much less effect on the Q-component. Computing the apparent conductivity, however, requires a value for the apparent magnetic susceptibility, which is calculated from I at the lowest frequency (typically <1 kHz) measured at a specific sensor height. Uncertainties in the sensor height, common with a handheld or cart-mounted sensor in rough terrain, can produce an error on the computed magnetic susceptibility; then the error is propagated to the apparent conductivity.

The quad–quad technique computes the apparent conductivity from the quadrature components at two frequencies. Paterson (1961) has developed a dual-frequency quadrature airborne electromagnetic (AEM) system in which the ratio of the quadrature component at the lower frequency to that at the higher one is used qualitatively to estimate the electrical property of the earth. The technique was necessary in 1961 because Q-component was easier to measure than I-component in the presence of a strong primary field. For the same reason, some current EM sensors measure the quadrature that can be transformed into apparent conductivity at low to middle induction numbers (McNeill, 1980, 1990). The transformation fails at middle to high induction numbers. Huang and Fraser (1998, 2002) define the quad–quad apparent resistivity for helicopter resistivity mapping in magnetic areas. Computed from Q-components at two frequencies, it is virtually immune to variations in magnetic susceptibility and sensor altitude. In this paper, we introduce a similar quad–quad conductivity for detecting buried metal objects such as UXO.

QUAD-QUAD CONDUCTIVITY

For a sensor with colocated transmitting and receiving coils (Figure 1), the half-space response can be expressed as a ratio of secondary magnetic field intensity H_2 to primary magnetic field intensity H_1 at the receiving coil (Ward and Hohmann,

Published on Geophysics Online June 29, 2004. Manuscript received by the Editor October 8, 2003; revised manuscript received March 22, 2004.
[1]Geophex, Ltd., 605 Mercury Street, Raleigh, North Carolina 27603-2343. E-mail: huang@geophex.com; ijwon@geophex.com.

1988):

$$\frac{H_2}{H_1} = a^2 \int_0^\infty R(\sigma\mu\omega\lambda)\lambda \exp(-2\lambda h) J_1(\lambda a) d\lambda, \qquad (1)$$

where a is the transmitter coil radius; h is the sensor height; J_1 is the Bessel function of the first kind of order one; R is a complex function of conductivity σ, magnetic permeability μ, angular frequency ω, and the variable of integration λ, which is the radial spatial wavenumber. For a homogeneous half-space, it can be expressed as

$$R(\sigma\mu\omega\lambda) = \left(\lambda - \frac{\sqrt{\lambda^2 + i\omega\sigma\mu}}{\mu_r}\right) \Bigg/ \left(\lambda + \frac{\sqrt{\lambda^2 + i\omega\sigma\mu}}{\mu_r}\right), \qquad (2)$$

where i is a unit of imagery number and μ_r is the relative magnetic permeability defined as μ divided by the permeability of free space, μ_0. Later, we use the more common magnetic susceptibility κ, defined as $\kappa = \mu_r - 1$.

The complex quantity H_2/H_1, when multiplied by 10^6, is in units of parts per million and consists of the real (I) and imaginary (Q) components. Equation 1 can be used to derive the traditional apparent conductivity based on the observed I and Q, hereafter called the I–Q-conductivity, at a particular frequency. The quad–quad apparent conductivity, hereafter called the Q–Q conductivity, is computed from the Q responses at two different frequencies f_L and f_H. The low- and high-frequency responses Q_L and Q_H can be combined to a single parameter such as the ratio Q_L/Q_H or amplitude $Q_L + Q_H$.

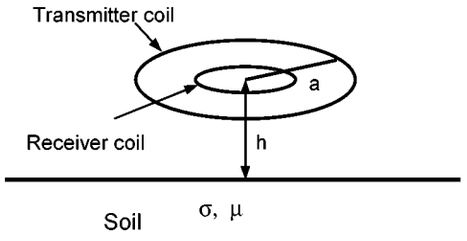

Figure 1. A concentric coil sensor over a half-space.

To derive the Q–Q conductivity, let us first define an amplitude A that is scaled by the sensor height h and coil radius a:

$$A = (Q_L + Q_H)\left(\frac{h}{a}\right)^3. \qquad (3)$$

Figures 2a and 2b show the ratio Q_L/Q_H and the scaled amplitude A as a function of induction number $\theta = (\omega\sigma\mu/2)^{1/2}h$ for various values of h/a over a homogeneous half-space. Neither the ratio nor the amplitude is overly sensitive to h/a at typical soil conditions where θ rarely exceeds 0.1. To determine the Q–Q conductivity, we take the following steps.

1) Determine Q_L/Q_H from the data on the y-axis in Figure 2a, select a suitable h/a curve for the data, and determine the corresponding θ on the x-axis.
2) In Figure 2b, locate the value of θ thus obtained on the x-axis and determine the corresponding A on the y-axis.
3) Compute the apparent sensor height h_a using Equation 3:

$$h_a = a\left(\frac{A}{Q_L + Q_H}\right)^{\frac{1}{3}}.$$

4) Obtain the Q–Q conductivity from $\theta = (\omega\sigma\mu/2)^{1/2}h$:

$$\sigma = \frac{\theta^2}{\pi f_L \mu h_a^2}, \qquad (4)$$

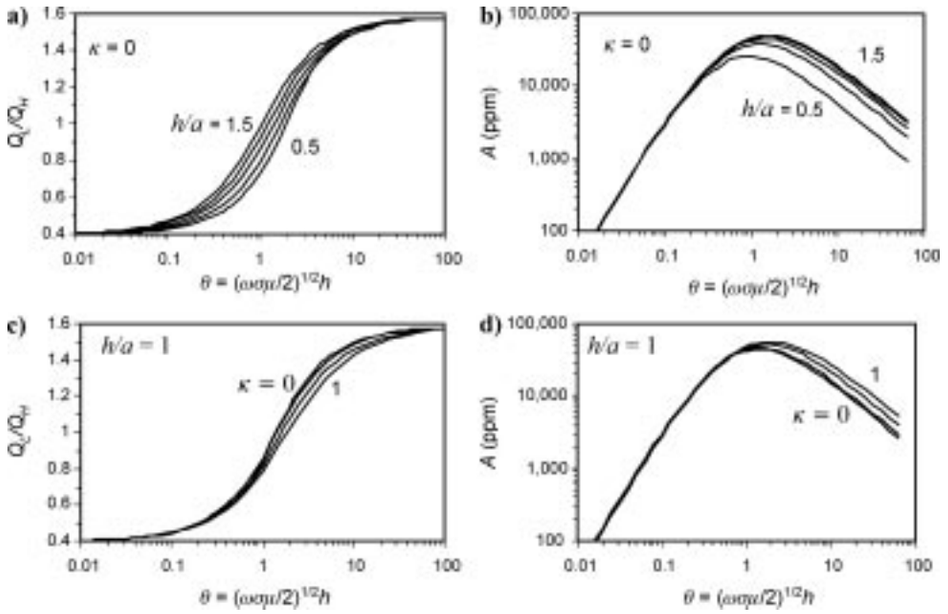

Figure 2. The ratio Q_L/Q_H (a, c) and a scaled amplitude A (b, d) as a function of induction number θ for various values of sensor height over a homogeneous half-space (a, b) and magnetic susceptibility (c, d). The frequency ratio f_H/f_L is 1.6.

where μ in equation 4 can be replaced by μ_0 since Q_L/Q_H and A are hardly affected by the change, as demonstrated in Figures 2c and 2d.

To illustrate the effect of h on apparent conductivity, we first compute the I and Q data for various h and κ. We then convert the data into the Q–Q conductivity as well as the I–Q conductivity assuming $h/a = 0.625$, typical for UXO surveys, using a GEM-3 sensor (Won et al., 1997; Won, 2003). Figure 3a shows the percent error for $\sigma f = 1000$ and $\kappa = 0.05$. For $0.2 < h/a < 1$, a reasonable range for a handheld sensor, the Q–Q conductivity is independent of h/a within 1%. The I–Q conductivity, on the other hand, is exact only when h/a is correct but is grossly wrong elsewhere. Errors in Q–Q conductivity from varying magnetic susceptibility κ are shown in Figure 3b—very small errors for the range of normal geologic materials.

The Q–Q conductivity can be wrong at large θ for helicopter EM data. Huang and Fraser (2002) suggest that the Q–Q conductivity should be used only when $\sigma f < 500$ over a conductive overburden or $\sigma f < 50$ over a conductive basement below a resistive cover, which corresponds to $\theta = 1.33$ or 0.42 for helicopter EM systems. For ground sensors with an upper frequency of 48 kHz, however, the error is negligible because θ rarely exceeds about 0.4 for normal soils. Figure 4 depicts the Q–Q conductivity for two-layer cases where the upper layer $\sigma_1 f = 1000$ and σ_2/σ_1 varies from 0.01 to 100.

Another issue concerning Q–Q conductivity is the ratio of the higher frequency to the lower frequency, f_H/f_L, which is set to 1.6 in the above examples. Figure 5 shows the effect of this frequency ratio between 1.2 and 12.8 for a fixed f_L. Notice that the Q–Q conductivity is fairly insensitive to the ratio.

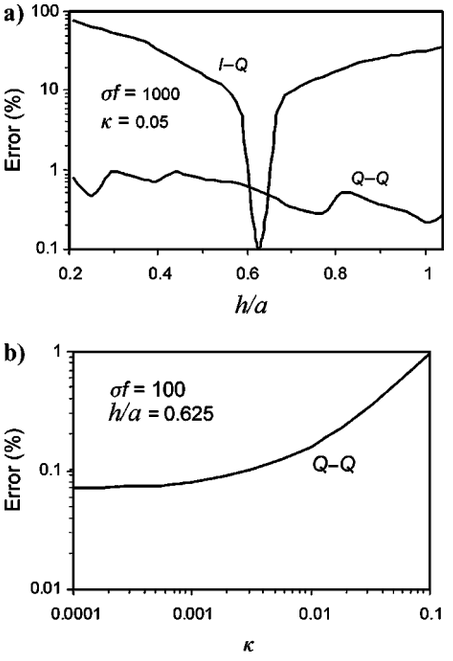

Figure 3. (a) The relative errors of the I–Q and Q–Q conductivities as a function of sensor height for $\sigma f = 1000$ and $\kappa = 0.05$. (b) The relative errors of Q–Q conductivity as a function of κ.

Q–Q CONDUCTIVITY FOR METAL OBJECTS

We now investigate the Q–Q conductivity for buried metal objects. A sphere is chosen as a model, mainly because its analytic solution is available. Consider a sphere of radius r, conductivity σ, and relative permeability μ_r, buried at depth z to its center. Figure 6 shows computed profiles of the Q–Q and I–Q conductivities of the sphere using EM data computed at 10 frequencies between 330 and 43 470 Hz, each of which is geometrically spaced at a factor of about 1.72. We first note that the Q–Q conductivity is much higher (>10 times) than the I–Q conductivity, indicating the Q–Q conductivity favors metal objects. For both Q–Q and I–Q, the amplitude is high at low frequency and decreases as the frequency increases.

Apparent conductivity of a metal object is proportional to the metal content and inversely proportional to the distance from the sensor to the object. The total apparent conductivity is a weighted average of apparent conductivities at all frequencies as defined by Huang and Won (2003c). As a single-parameter detector function, let us define the total Q–Q apparent

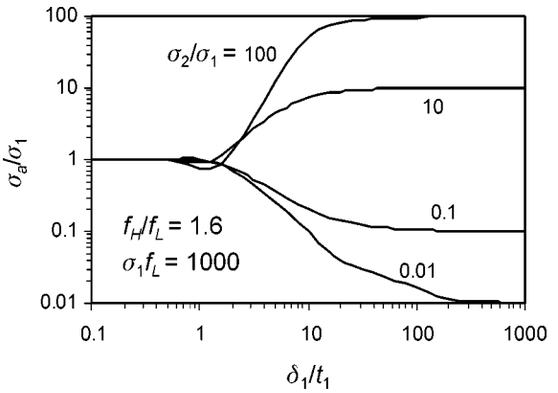

Figure 4. The Q–Q conductivity for two-layer cases as a function of the ratio of the skin depth δ_1 in the upper layer to the upper-layer thickness t_1. The product of frequency and conductivity of the upper layer $\sigma_1 f$ is fixed at 1000, and σ_2/σ_1 varies from 0.01 to 100.

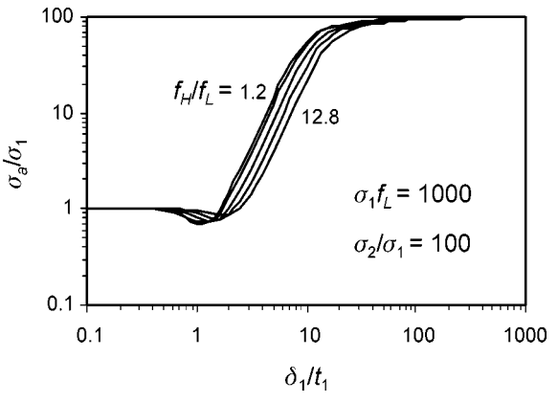

Figure 5. The Q–Q conductivity for two-layer cases as a function of δ_1/t_1 for various frequency ratios f_H/f_L, where $\sigma_1 f = 1000$ and $\sigma_2/\sigma_1 = 100$.

conductivity as

$$TAC_{QQ} = \frac{\sum_{i=1}^{N-1} \frac{\sigma_a(Q_i, Q_{i+1})}{\log(f_i)}}{\sum_{i=1}^{N-1} \frac{1}{\log(f_i)}}, \qquad (5)$$

where N is the number of frequencies and $\sigma_a(Q_i, Q_{i+1})$ is the Q–Q apparent conductivity computed from frequencies f_i and f_{i+1}. As noted in equation 5, TAC_{QQ} is a single detection indicator formed by a weighted average of all Q–Q conductivities. Figure 7 shows amplitudes of the total apparent conductivity and relative sensitivity of Q–Q conductivity as a function of normalized depths to the center of the sphere. The Q–Q conductivity has not only a higher amplitude but also a smaller rate of decrease with the depth. As shown in Figure 7b, the relative sensitivity of the Q–Q conductivity, which is defined as the ratio of the Q–Q amplitude to the I-Q amplitude, is proportional to the ratio of target depth to target size. Therefore, detection for smaller or deeper targets may be better for the Q–Q technique than for the I–Q technique.

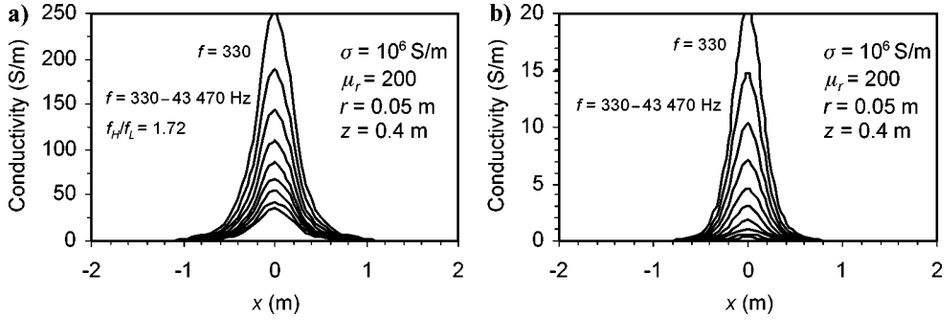

Figure 6. Profiles of the (a) Q–Q and (b) I–Q conductivities of a sphere inverted from EM data at 10 frequencies between 330 Hz and 43 470 Hz spaced approximately by a factor of 1.72.

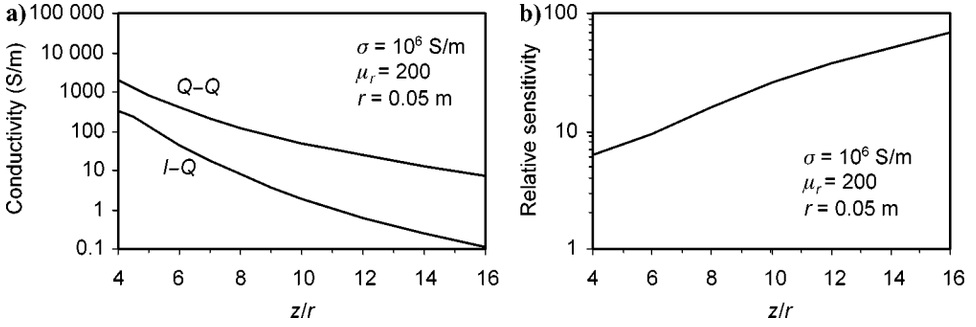

Figure 7. (a) Amplitudes of the total apparent conductivity computed from both Q–Q and I–Q techniques and (b) relative sensitivity of Q–Q conductivity as a function of depths to the center of the sphere.

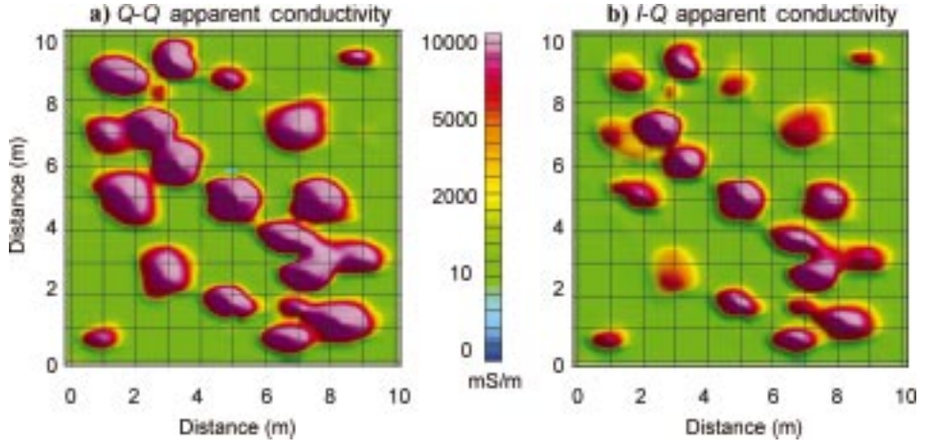

Figure 8. (a) Q–Q and (b) I–Q conductivities derived from the Geophex test site data, showing anomalies from 21 buried metal pipes. As expected, a buried diabase boulder at (0.5,4) did not produce an anomaly.

FIELD EXAMPLES

The first example comes from GEM-3 data obtained at a test site constructed by Geophex in Raleigh, North Carolina. The soil is dense, red clay with moderate conductivity (10–20 mS/m) and susceptibility (~0.001). The 10 × 10-m site contains 21 metal pipes of various diameter and length. The site also contains a diabase boulder, a magnetic rock. Further site descriptions can be found in Huang and Won (2003a,c).

We used a handheld GEM-3 sensor with a 20-cm radius coil for this data. In an effort to simulate practical field conditions, we followed a common survey practice often called dead reckoning: an operator with a hand-held GEM-3 walked steadily toward an end-of-the-line marker (typically a traffic cone) while

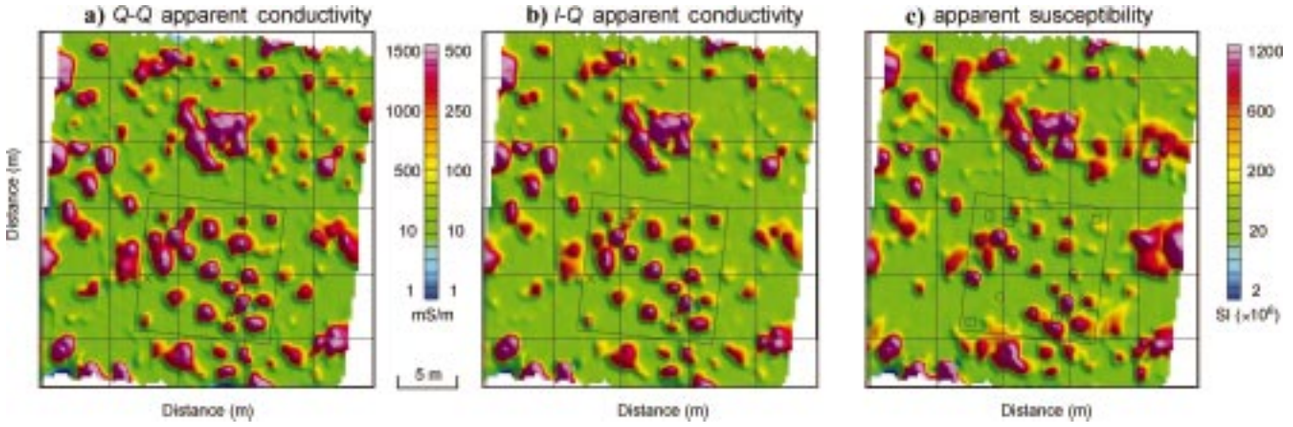

Figure 9. (a) *Q*–*Q* and (b) *I*–*Q* conductivities and (c) residual magnetic susceptibility derived from the data obtained at the Geophex test site (indicated by frame) and the surrounding area using a cart-mounted GEM-3 sensor. Circles—steel pipes; squares—nonferrous pipes; the triangle—20-mm projectile buried temperately; cross—magnetic rock.

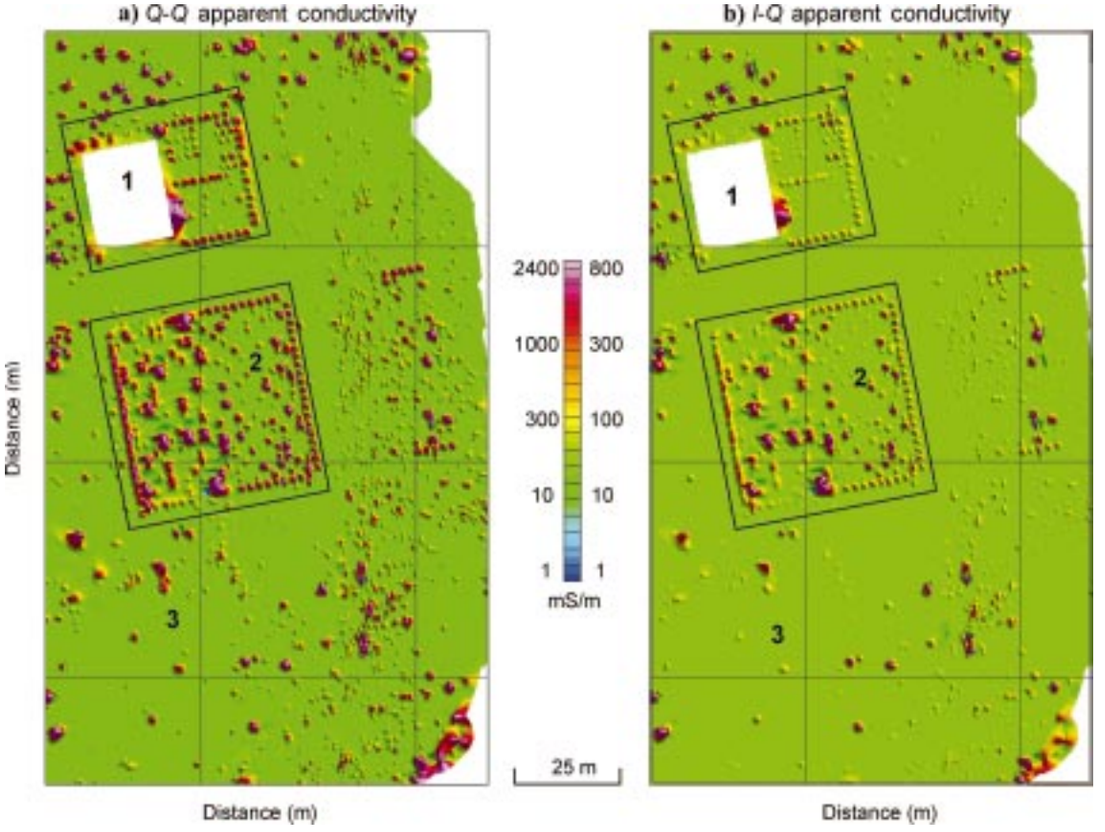

Figure 10. Maps of (a) *Q*–*Q* and (b) *I*–*Q* conductivities over a 100 × 170-m grid in the Standardized UXO Technology demonstration site at Aberdeen, Maryland. Numbered areas devote (1) calibration lanes, (2) the blind test grid, and (3) part of the open-rood terrain.

visually maintaining the sensor height at about 20 cm above the ground. The GEM-3 collected 10 data points per second, which resulted in a data interval of about 5 cm for a typical walking speed. The data obtained over each line was then equally distributed along the line, assuming that the walking speed was constant and the line was straight. Position errors for such data could be as high as 20 cm because of uneven walking speed and a crooked path. Likewise, the sensor height might vary more than 10 cm. Figure 8 shows the total Q–Q and I–Q conductivities using four frequencies in a bandwidth from 90 Hz to 5430 Hz. The total I–Q conductivity is a weighted average over four frequencies, while the total Q–Q conductivity is a weighted average of three frequency pairs. Both maps show all seeded targets with a quiet background, but the Q–Q conductivity shows higher amplitudes over all targets. As expected, the magnetic rock located at (0.5,4) does not appear on either map.

Figure 9 shows the maps of Q–Q and I–Q conductivities as well as the apparent susceptibility from an in-phase component at 90 Hz from the same location but including the surrounding area. The data were obtained using a cart-mounted GEM-3 with a 48-cm radius coil, along with differential GPS navigation, with 0.5-m line intervals. The total conductivities were computed from eight frequencies in a bandwidth of 150 to 23 850 Hz. The anomalies on the Q–Q conductivity map are much stronger than those on the I–Q map. Ferrous metal objects are indicated by both the conductivity and susceptibility maps, nonferrous targets only by the conductivity map, and magnetic rock only by the magnetic susceptibility map.

The second example is from the Standard UXO Technology demonstration site at Aberdeen Proving Grounds (APG), Maryland. It is a seeded site for controlled testing and includes (1) calibration lanes for system training and target characterization and a set of blind areas for testing a range of scenarios; (2) a blind test grid—a 1600-m^2 rectangular grid including access lanes separating 400 discrete 1×1-m-square interrogation points; (3) open-road terrain—a large area that can be surveyed with vehicular towed systems over some moderately varied rough terrain; (4) moguls—an area with moguls and craters of about ± 1 m vertical relief, requiring manual data acquisition, likely in a handheld sensor configuration; and (5) a wooded area with various vegetation and dense trees.

Figure 10 presents the total Q–Q and I–Q conductivity maps, which include calibration lanes, the blind test grid, and part of the open-road terrain. The GEM-3 data were collected at 10

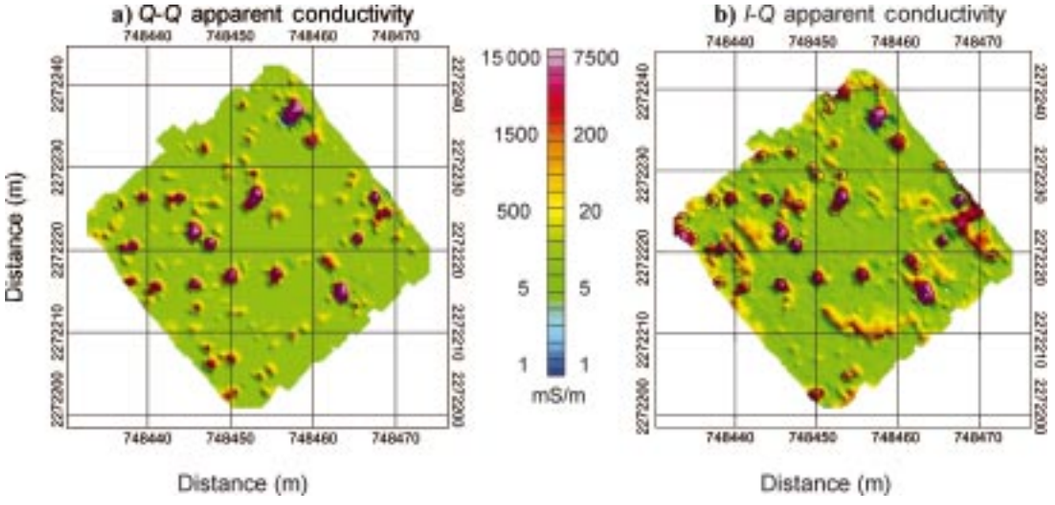

Figure 11. Maps of (a) Q–Q and (b) I–Q conductivities over a 30×30-m grid in Kaho'olawe, Hawaii, showing greater geologic noise in the latter.

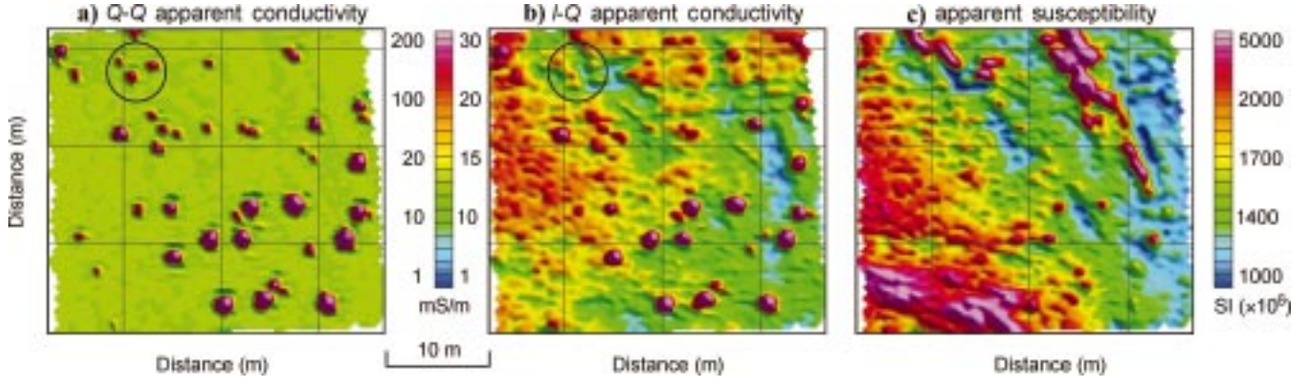

Figure 12. Maps of (a) Q–Q and (b) I–Q conductivities and (c) magnetic susceptibility derived from the data obtained at the California site.

frequencies from 90 Hz to 40 kHz using a sled-mounted sensor with a 48-cm radius sensing head. The sled was towed by an all-terrain vehicle (ATV). Line spacing varied from 0.2 to 2 m. The area is relatively flat, so variations in soil magnetic susceptibility or sensor height did not affect the EM data significantly. The advantage of Q–Q conductivity in such areas is that anomalies from deep or small targets may have a better chance of being detected. Some seeded targets in calibration lanes and the blind test grid are missing because the targets are too small or deep beyond the sensor's detection capacity and because the line spacing is too large (2 m).

The last two examples are from Kaho'olawe, Hawaii, where the volcanic geology results in highly magnetic soils, and from an army site in California with an outcrop of magnetic rocks. A cart-mounted GEM-3 sensor with differential GPS collected the EM data at 10 frequencies (90 Hz–40 kHz).

Figure 11 shows the total Q–Q and I–Q conductivity maps from Kaho'olawe. In comparison with the I–Q map, the Q–Q map is less cluttered with noise related to variations in sensor height over magnetic geology. Therefore, it better shows metallic targets, as indicated by higher values in the apparent conductivity.

Figure 12 shows maps of total Q–Q, I–Q conductivity, and magnetic susceptibility from the California site. This 30×30-m area is of rough terrain because of outcrops. Features in magenta on the magnetic susceptibility map are outcrops of magnetic bedrock. It is obvious that the I–Q conductivity is affected by variations in the sensor height or terrain magnetic susceptibility. For example, three anomalies at the northwest of the grid on the Q–Q conductivity map (in the circle) are barely recognized on the I–Q conductivity map.

CONCLUSIONS

We have introduced the Q–Q conductivity method for detecting buried metal objects in magnetic terrains and have compared its properties against traditional I–Q conductivity. Our study indicates that certain issues of Q–Q conductivity encountered in helicopter EM surveys (using a layered earth as the model) do not exist in ground surveys using a small EM sensor searching for isolated metal objects.

Compared with traditional I–Q conductivity, the Q–Q technique has the following advantages: it is insensitive to magnetic soils and sensor motions and is biased toward metal objects. The Q–Q conductivities are sensitive to small and/or deep metal objects, while the technique suppresses the background noise caused by sensor motion over, and susceptibility variations in, magnetic soils.

ACKNOWLEDGMENTS

This study has been partly funded by the Department of Defense Strategic Environmental Research and Development Program (SERDP) in Arlington, Virginia, and partly by the U.S. Army Night Vision Laboratory Countermine Division, Fort Belvoir, Virginia.

REFERENCES

Huang, H., and D. C. Fraser, 1998, Magnetic permeability and electric resistivity mapping with a multifrequency airborne EM system: Exploration Geophysics, **29**, 249–253.

——— 2002, The use of quad–quad resistivity in helicopter electromagnetic mapping: Geophysics, **67**, 459–467.

Huang, H., and I. J. Won, 2000, Conductivity and susceptibility mapping using broadband electromagnetic sensors: Journal of Environmental and Engineering Geophysics, **5**, No. 4, 31–41.

——— 2003a, Characterization of UXO-like targets using broadband electromagnetic induction sensors: IEEE Transactions on Geoscience and Remote Sensing, **41**, No. 3, 652–663.

——— 2003b, Detecting metal objects in magnetic environments by broadband electromagnetic method: Geophysics, **68**, 1877–1887.

——— 2003c, Automated anomaly picking from broadband electromagnetic data in UXO survey: Geophysics, **68**, 1870–1876.

McNeill, J. D., 1980, Electromagnetic terrain conductivity measurements at low induction numbers: Technical Note TN-6, Geonics Limited.

——— 1990, Use of electromagnetic methods for groundwater studies, *in* S. H. Ward, Ed., Geotechnical and environmental geophysics: Society of Exploration Geophysicists, 191–218.

Paterson, N. R., 1961, Experimental and field data for the dual-frequency phase-shift method of airborne electromagnetic prospecting: Geophysics, **26**, 601–617.

Ward, S. H., and G. W. Hohmann, 1988, Electromagnetic theory for geophysical applications, *in* M. N. Nabighian, Ed., Electromagnetic methods in applied geophysics: Society of Exploration Geophysicists, 130–311.

Won, I. J., 2003, Small frequency-domain electromagnetic induction sensors: The Leading Edge, **22**, 320–322.

Won, I. J., and H. Huang, 2004, Magnetometers and electromagnetometers: The Leading Edge, **23**, 448–451.

Won, I. J., D. A. Keiswetter, D. R. Hanson, E. Novikova, and T. M. Hall, 1997, GEM-3: A monostatic broadband electromagnetic induction sensor: Journal of Environmental and Engineering Geophysics, **2**, No. 1, 53–64.